ARTICLE

Enhanced Mechanical Properties of Nanocomposites at Low Graphene Content

Mohammad A. Rafiee,[†] Javad Rafiee,[†] Zhou Wang,[‡] Huaihe Song,[‡] Zhong-Zhen Yu,[‡] and Nikhil Koratkar[†,*]

[†]Department of Mechanical, Aerospace and Nuclear Engineering, Rensselaer Polytechnic Institute, 110 Eighth Street, Troy, New York 12180-3590, and [‡]State Key Laboratory of Chemical Resource Engineering, College of Materials Science and Engineering, Beijing University of Chemical Technology, Beijing 100029, China

ABSTRACT In this study, the mechanical properties of epoxy nanocomposites with graphene platelets, single-walled carbon nanotubes, and multi-walled carbon nanotube additives were compared at a nanofiller weight fraction of 0.1 ± 0.002%. The mechanical properties measured were the Young's modulus, ultimate tensile strength, fracture toughness, fracture energy, and the material's resistance to fatigue crack propagation. The results indicate that graphene platelets significantly out-perform carbon nanotube additives. The Young's modulus of the graphene nanocomposite was ~31% greater than the pristine epoxy as compared to ~3% increase for single-walled carbon nanotubes. The tensile strength of the baseline epoxy was enhanced by ~40% with graphene platelets compared to ~14% improvement for multi-walled carbon nanotubes. The mode I fracture toughness of the nanocomposite with graphene platelets showed ~53% increase over the epoxy compared to ~20% improvement for multi-walled carbon nanotubes. The fatigue resistance results also showed significantly different trends. While the fatigue suppression response of nanotube/epoxy composites degrades dramatically as the stress intensity factor amplitude is increased, the reverse effect is seen for graphene-based nanocomposites. The superiority of graphene platelets over carbon nanotubes in terms of mechanical properties enhancement may be related to their high specific surface area, enhanced nanofiller—matrix adhesion/interlocking arising from their wrinkled (rough) surface, as well as the two-dimensional (planar) geometry of graphene platelets.

KEYWORDS: epoxy nanocomposites · graphene platelets · mechanical properties · single-walled carbon nanotubes · multi-walled carbon nanotubes

Graphene is a single-atom-thick sheet of sp^2-hybridized carbon atoms.[1] Graphene can be produced by four methods: (1) chemical vapor deposition;[2] these studies which began in the 1970s were followed by a substantial body of work by surface scientists on monolayer graphite;[3] (2) epitaxial growth of graphene films on electrically insulating substrates;[4] (3) mechanical exfoliation of graphene from bulk graphite (*e.g.*, using Scotch tape[5]); and (4) reduction of graphene derivatives such as graphene oxide.[6,7] The last method shows potential for the production of graphene sheets in the bulk quantities that are necessary for application to composites. Graphene oxide sheets can be extracted from "graphite oxide", which is typically prepared by the oxidation of graphite.[8−10] Graphite oxide can be completely exfoliated to produce aqueous colloidal suspensions of graphene oxide sheets by sonication.[1] Considerable research[11,12] on such aqueous colloidal suspensions was carried out in the 1950s and the 1960s. Chemical reduction of graphene oxide in colloidal suspensions can be performed to generate bulk quantities of chemically modified graphene (CMG) sheets[1,13] that are suitable for composite applications. Thermal reduction of graphite oxide is another approach that can be used to obtain bulk quantities of graphene platelets. Rapid heating (>2000 °C/min) up to 1050 °C exfoliates as well as reduces graphite oxide.[1,14,15] Thermal reduction of graphite oxide is the method that we have utilized in the present study to produce gram quantity of graphene platelets (GPL). Note that the term platelet is used here instead of sheet to clarify that GPL is not a single (individual) graphene sheet but comprises multiple graphene sheets that are stacked together. The thickness of GPL is therefore significantly larger than an individual graphene sheet.

Graphene building blocks can be used to construct a variety of carbon-based nanostructures. For example, such a sheet can be rolled up seamlessly to generate a single-walled carbon nanotube (SWNT). Multiple concentric SWNT cylinders which share a common axis comprise multi-walled carbon nanotubes (MWNT). All of the above nanostructures are endowed with excellent mechanical properties (such as modulus and strength) due to the sp^2 carbon bonding network that is common to SWNT, MWNT, and graphene. A key question is which of these nanofillers is best suited to transferring their mechanical properties to the polymer matrix in nanocomposites.

*Address correspondence to koratn@rpi.edu.

Received for review August 20, 2009 and accepted November 13, 2009.

Published online December 3, 2009. 10.1021/nn9010472

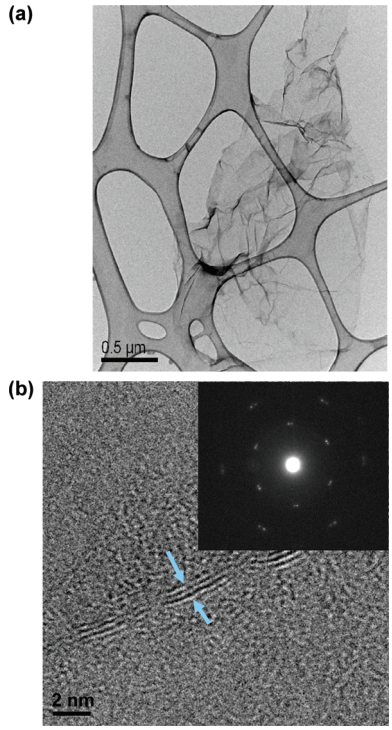

Figure 1. (a) TEM image of a GPL flake deposited on a standard TEM grid, and (b) HRTEM image of the edges of a GPL flake indicating the layered graphene platelet structure. The inset shows the measured electron diffraction pattern.

To investigate this, we compared the Young's modulus, tensile strength, fracture toughness, fracture energy, and the material's resistance to fatigue crack propagation for epoxy nanocomposites at a fixed weight fraction (0.1 ± 0.002%) of SWNT, MWNT, and graphene platelet (GPL) fillers. We intentionally selected a low weight fraction of ~0.1% to ensure relatively uniform dispersion of the SWNT, MWNT, and GPL in the epoxy matrix. The Young's modulus of the GPL and carbon nanotube composites was also compared with the predictions of the well-established Halpin–Tsai model. Our results indicate that, at low nanofiller content, GPL nanocomposites offer significant improvement in mechanical properties as compared to carbon nanotube composites.

The GPLs used in this study were prepared by the thermal reduction of graphite oxide (Materials and Methods).[14,15] Figure 1a illustrates a transmission electron microscopy (TEM) image of a GPL flake synthesized by the above method and deposited on a standard TEM grid for imaging. The flake dimensions are ~2.5 μm × 1.5 μm; note the wrinkled surface texture of the GPL, which could play an important role in enhancing mechanical interlocking and load transfer with the matrix.[13,16] Figure 1b shows high-resolution transmission electron microscopy (HRTEM) and electron diffraction pattern images of the GPL indicating the layered graphene structure within the platelet. The GPL flakes used in our study are composed of such stacked individual graphene sheets.

The approach used to disperse GPL in a bisphenol-A-based thermosetting epoxy[17,18] is shown schematically in Figure 2a and is discussed in detail in the Materials and Methods. Both compact tension samples for crack propagation study and dog-bone-shaped specimens for uniaxial tensile testing were fabricated and tested. Figure 2b shows a scanning electron microscopy (SEM) image of a freeze-fractured nanocomposite sample with ~5% weight of GPL. The image clearly indicates epoxy-coated GPL flakes that are protruding out of the fracture surface of the sample. The inset in Figure 2b depicts a high-resolution SEM image indicating the wavy edge structure of the GPL. Note that at low weight fractions of GPL (below 0.5%) it was quite challenging to study the GPL dispersion by SEM analysis due to the planar geometry of the GPL and the epoxy coating on the GPL, which allows only the exposed platelet edges to be discernible. The single-walled carbon nanotubes (SWNT, purity >95%) used in this study were provided by Cheap Tube Inc. with a mean diameter of 2 nm and length of 10 μm. Multi-walled carbon nanotubes (MWNT, purity >95%) were provided by Nanocyl with a mean diameter of 20 nm and length of 20 μm. The protocols used to disperse the carbon nanotubes in the epoxy matrix are described in detail elsewhere.[17–19]

The results of uniaxial tensile testing of the baseline epoxy and nanocomposite samples are shown in Figure 3a,b. To check for reproducibility of the results, at least four samples of each group were fabricated and tested. The weight fraction of GPL, SWNT, and MWNT in the epoxy matrix was held constant at 0.1 ± 0.002%. Since dispersion of two-dimensional sheets can be significantly more challenging as compared to one-dimensional fibers, a low nanofiller weight fraction of ~0.001 (*i.e.*, 0.1%) was selected to ensure relatively uniform dispersion. Figure 3a shows the ultimate tensile strength measurements for the pure epoxy and the nanocomposite samples. Clearly, the GPL additives far out-perform the SWNT and MWNT fillers. The tensile strength of the GPL/epoxy nanocomposite (~78 MPa) is about 40% larger than the pristine epoxy (~55 MPa). The fact that this is achieved at a nanofiller weight fraction of ~0.1% is impressive. By contrast, SWNT/epoxy and MWNT/epoxy composites show ~11 and ~14% increase, respectively, in the tensile strength compared to the baseline epoxy matrix. Figure 3b compares the Young's modulus of the pristine epoxy and nanocomposite samples. Incorporation of 0.1 ± 0.002% weight fraction of GPL increases the Young's modulus of the baseline epoxy by ~31% from ~2.85 to ~3.74 GPa. The modulus enhancements for SWNT and MWNT composites at the same weight fraction of ~0.1% are significantly lower (<3%).

The well-established Halpin−Tsai model for fiber-reinforced composites was utilized to predict the Young's modulus of the nanocomposites. The SWNT and MWNT nanocomposites were considered as randomly oriented discontinuous fiber lamina;[20] the modulus of the composite can be calculated from the equation:

$$E_C = \frac{3}{8}\frac{1+2\left(\frac{l_{NT}}{d_{NT}}\right)\left(\frac{(E_{eq}/E_M)-1}{(E_{eq}/E_M)+2(l_{NT}/d_{NT})}\right)V_{NT}}{1-\left(\frac{(E_{eq}/E_M)-1}{(E_{eq}/E_M)+2(l_{NT}/d_{NT})}\right)V_{NT}} \times \frac{1+2\left(\frac{(E_{eq}/E_M)-1}{(E_{eq}/E_M)+2}\right)V_{NT}}{1-\left(\frac{(E_{eq}/E_M)-1}{(E_{eq}/E_M)+2}\right)V_{NT}} \times E_M + \frac{5}{8} \times E_M \quad (1)$$

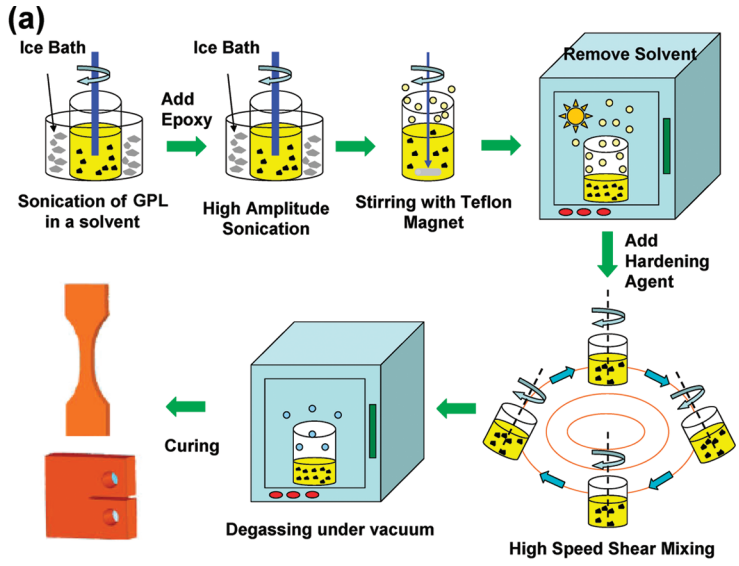

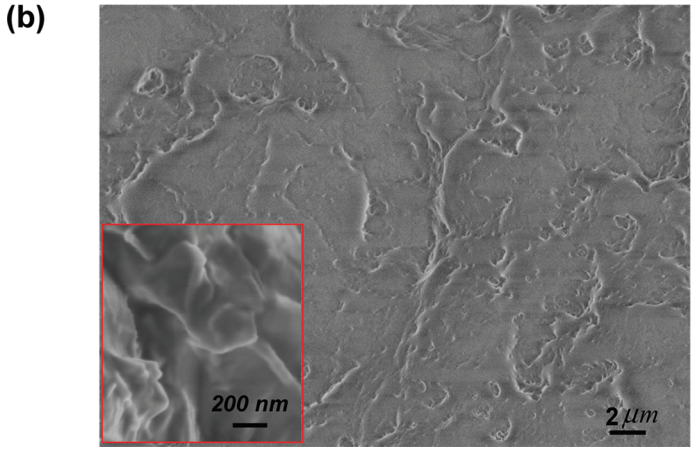

Figure 2. (a) Schematic showing the dispersion of graphene sheets in the epoxy matrix *via* solution mixing with high amplitude ultrasonic agitation and high-speed shear mixing. (b) SEM analysis of the freeze-fractured surface of a graphene/epoxy composite (with ~5% weight of GPL) indicating epoxy-coated GPL flakes protruding out of the fracture surface. Inset shows a high-resolution SEM image indicating the wavy edge structure of the GPL.

where E_C = Young's modulus of the composite, l_{NT} = length of nanotube (l_{SWNT} = 10 μm, l_{MWNT} = 20 μm), d_{NT} = average outer diameter of nanotube (d_{SWNT} = 2 nm, d_{MWNT} = 20 nm), E_{NT} = Young's modulus of the nanotubes (E_{SWNT} = 1 TPa, E_{MWNT} = 450 GPa),[21] E_M = Young's modulus of the epoxy matrix, $E_{eq} = (2t/r^{NT})E_{NT}$ is equivalent modulus of the nanotube considering the hollow tube as a solid cylinder,[22] t = nanotube wall thickness (t^{SWNT} = 0.34 nm, t^{MWNT} = 1.5 nm), r^{NT} = nanotube radius (r^{SWNT} = 1 nm, r^{MWNT} = 10 nm), V_{NT} = volume content of the nanotubes (V_{SWNT} = 0.171 vol %, V_{MWNT} = 0.138 vol %). The volume content of the nanotubes was calculated according to the procedure shown in ref 23. The SWNT and MWNT density was estimated based on the known density of graphite (2.25 g/cm^3) and the manufacturer supplied nanotube diameters ($d_{outer,SWNT}$ = 2 nm, $d_{inner,SWNT}$ = 1.66 nm, $d_{outer,MWNT}$ = 20 nm, $d_{inner,MWNT}$ = 17 nm). The density of the epoxy matrix was determined to be ~1.2 g/cm^3.

To model the elastic modulus of the GPL nanocomposites, we assumed that graphene platelets (see Figure 1a,b) act as an effective rectangular solid fiber with width (W), length (L), and thickness (t). To predict elastic properties, the Halpin−Tsai equations[20,23,24] were modified for the GPL/epoxy nanocomposite as follows:

$$E_C = \frac{3}{8}\frac{1+\xi\eta_L V_{eff,fib}}{1-\eta_L V_{eff,fib}} \times E_M + \frac{5}{8}\frac{1+2\eta_W V_{eff,fib}}{1-\eta_W V_{eff,fib}} \times E_M \quad (2)$$

$$\eta_L = \frac{(E_{eff,fib}/E_M)-1}{(E_{eff,fib}/E_M)+\xi} \quad (3)$$

$$\eta_W = \frac{(E_{eff,fib}/E_M)-1}{(E_{eff,fib}/E_M)+2} \quad (4)$$

where E_C is the composite elastic modulus, $V_{eff,fib}$ is volume fraction of the effective fiber, and $E_{eff,fib}$ and E_M are the effective fiber and matrix moduli, respectively. $E_{eff,fib}$ is assumed as the GPL modulus (~1.01 TPa). The parameter ξ depends on the geometry and boundary conditions of the effective fiber. According to Halpin and Thomas[24,25] for rectangular filaments, the parameter ξ can be expressed as

$$\xi = 2\left(\frac{(W+L)/2}{t}\right) \quad (5)$$

where L, W, and t represent the average GPL length, width, and thickness. Hence, the nanocomposite elastic modulus can be defined in terms of the epoxy matrix properties and the GPL reinforcement. Assuming $V_{eff,fib} = V_{GPL}$ and by substituting eqs 3, 4, and 5 into 2 we have

$$E_C = \frac{3}{8}\frac{1+((W+L)/t)\left(\frac{(E_{GPL}/E_M)-1}{(E_{GPL}/E_M)+(W+L)/t}\right)V_{GPL}}{1-\left(\frac{(E_{GPL}/E_M)-1}{(E_{GPL}/E_M)+(W+L)/t}\right)V_{GPL}} \times E_M + \frac{5}{8}\frac{1+2\left(\frac{(E_{eff,fib}/E_M)-1}{(E_{eff,fib}/E_M)+2}\right)V_{GPL}}{1-\left(\frac{(E_{eff,fib}/E_M)-1}{(E_{eff,fib}/E_M)+2}\right)V_{GPL}} \times E_M \quad (6)$$

where, E_C is the elastic modulus of the nanocomposite. The density of the GPL and epoxy should be known in order to convert weight fraction to volume fraction, required to predict the elastic properties. For fibrous composites, the fiber volume fraction can be calculated using the density of the constituents:

$$V_{GPL} = \frac{\rho_C}{\rho_{GPL}} W_{GPL};\ \rho_C = \rho_{GPL}V_{GPL} + \rho_M V_M \quad (7)$$

where V_{GPL} and W_{GPL} are the volume and weight fraction of GPL, V_M is the volume fraction of the matrix, ρ_C is the density of composite, ρ_{GPL} is the GPL density, and ρ_M is the matrix density. By rearranging eq 7, the volume fraction can be expressed as follows:

$$V_{GPL} = \frac{W_{GPL}}{W_{GPL} + (\rho_{GPL}/\rho_M)(1 - W_{GPL})} \quad (8)$$

Figure 1b shows the top view HRTEM of the GPL edges showing the layered platelet structure. The interlayer spacing ($t' \approx 0.72$ nm) of the graphene platelets was directly measured from the micrograph by image processing techniques. This enables the GPL density to be estimated by appropriately scaling the density of fully dense graphite ($\rho_{graphite} = 2.25$ g/cm^3) with $t' \approx 0.34$ nm for the interlayer spacing in graphite. Using this approach, the GPL density was estimated as $\rho_{GPL} \approx 1.06$ g/cm^3. The estimated volume fraction for 0.1% weight of GPL then computes to $V_{GPL} = 0.112$ vol %. The theoretical prediction from eq 6 (with $L \approx 2.5$ μm, $W \approx 1.5$ μm, $t \approx 1.5$ nm) is ~3.23 GPa (Figure 3b), which under-predicts by ~13% the experimental results. This could be a consequence of the wrinkled (wavy) structure of the GPL, which is different from the rectangular shape of the GPL assumed by the model. The predictions of the Halpin−Tsai model for MWNT and SWNT epoxy nanocomposites are also shown in Figure 3b; for nanotube composites, the theory overpredicts the test data by up to 12%.

Finally, we investigated the fracture and the fatigue response of the nanotube and GPL/epoxy composites. Crack opening tests on compact tension samples (Materials and Methods) were performed to measure the mode I fracture toughness (K_{Ic}); the tests were conducted using a MTS-858 material testing system following ASTM standard D5045. An initial precrack was created in the compact tension samples by gently tapping a fresh razor blade over a molded starter notch. The radius at the tip of the precrack was similar for all of the samples tested, which was confirmed by optical microscopy prior to testing. At each weight fraction of GPL additives, we tested between 4 and 6 different samples to check for reproducibility of the results. Figure 4a indicates that compared to the epoxy the SWNT, MWNT, and GPL nanocomposites show ~14, ~20 and ~53% increase, respectively, in fracture toughness (K_{Ic}). For the fracture energy (G_{Ic}), we find 45, 66, and 126% enhancement for the SWNT, MWNT, and GPL nanocomposites, respectively (Figure 4a). The ability of the GPL in toughening the matrix is clearly superior to carbon nanotubes. This is also corroborated by the work of other groups. For example, previous studies have reported increases of only 18 and 26%

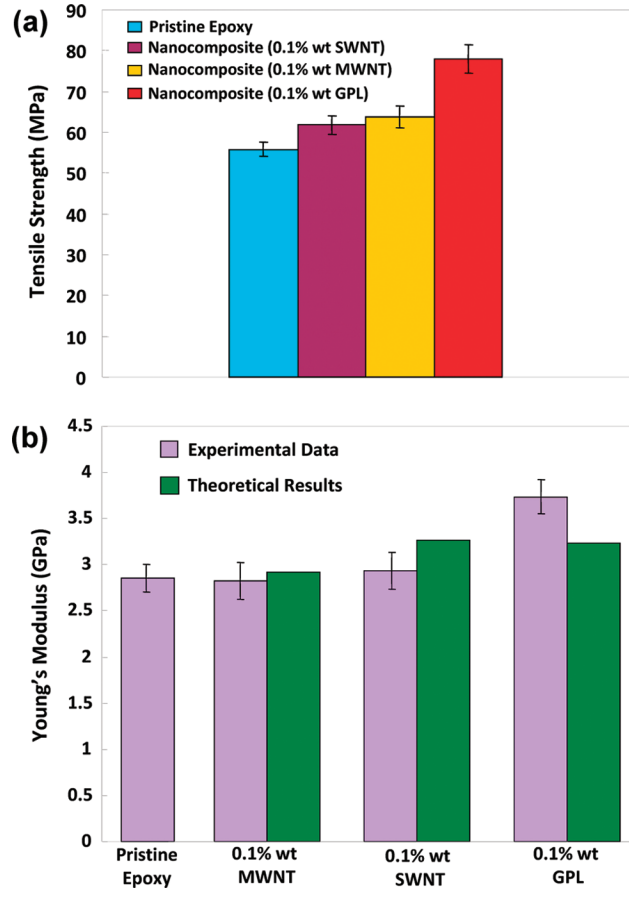

Figure 3. Uniaxial tensile testing. (a) Ultimate tensile strength for the baseline epoxy and GPL/epoxy, MWNT/epoxy, and SWNT/epoxy nanocomposites. The weight fraction of nanofillers for all of the nanocomposite samples tested was fixed at ~0.1%. (b) Young's modulus of nanocomposite samples with ~0.1% weight of GPL, ~0.1% weight of SWNT, and ~0.1% weight of MWNT is compared with the pristine (*i.e.*, unfilled) epoxy matrix. Theoretical predictions using the Halpin−Tsai theory for the nanocomposite samples are also shown in the figure. The error in estimation of weight fraction for the various nanocomposite samples is estimated to be less than ±0.002%.

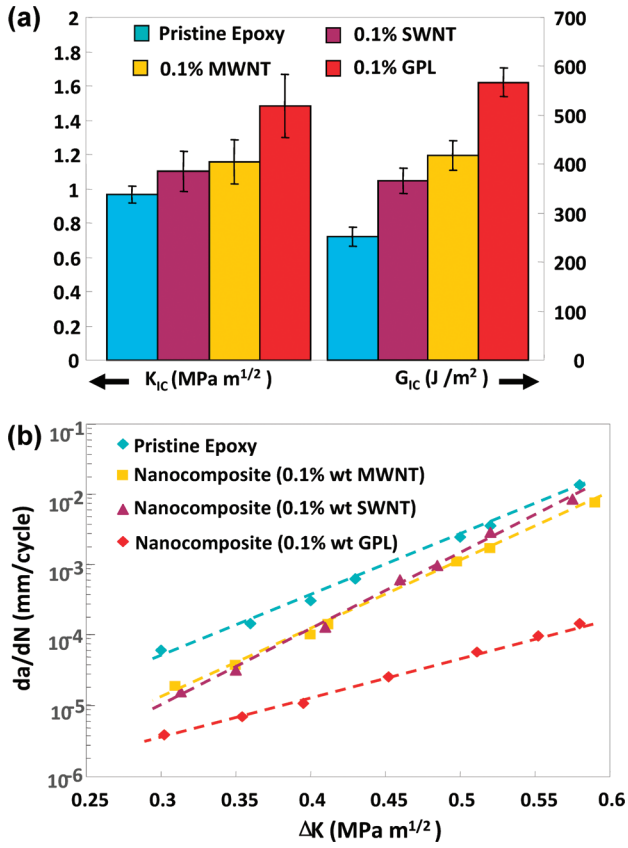

Figure 4. Fracture and fatigue testing. (a) Mode I fracture toughness (K_{Ic}) and fracture energy (G_{Ic}) for the baseline epoxy and GPL/epoxy, MWNT/epoxy, and SWNT/epoxy nanocomposites at ~0.1 wt % fraction of nanofillers. (b) Fatigue crack propagation testing; crack growth rate (d*a*/d*N*) plotted as a function of the stress intensity factor amplitude (ΔK) for the pristine epoxy and nanocomposite samples with ~0.1 wt % of GPL, ~0.1 wt % of SWNT, and ~0.1 wt % of MWNT additives. The error in estimation of weight fraction for the various nanocomposite samples is estimated to be less than ±0.002%.

in the fracture toughness of epoxy composites with 0.1 and 1 wt %, respectively, of amine-functionalized double-walled carbon nanotubes.[26] The fracture toughness of GPL is also impressive in relation to nanoparticle composites. For example, the weight fraction of SiO_2 nanoparticles (~7.8%) required[27] to increase the fracture toughness of the neat epoxy by 54% is nearly *80-fold higher* compared to GPL. Similarly, clay nanocomposites require between 5 and 10 wt % of nanoclay additives in various epoxy resins to achieve a 60% increase in the fracture toughness,[28] which is *50- to 100-fold larger* than the GPL weight fraction of 0.1%.

To evaluate the composite's performance under fatigue conditions, dynamic crack propagation tests on compact tension samples were conducted following ASTM E647 standard (details provided in the Materials and Methods). Figure 4b shows the measured crack propagation rate (d*a*/d*N*) *versus* the applied stress intensity factor amplitude (ΔK). A substantial lowering in the crack growth rate over the full range of stress intensity factor amplitudes can be observed for the GPL nanocomposite compared to the baseline epoxy. For example, at $\Delta K = 0.5$ MPa $m^{1/2}$, the d*a*/d*N* for the nanocomposite (5.87×10^{-5} mm/cycle) is ~40-fold lower than the baseline epoxy (2.5×10^{-3} mm/cycle). Figure 4b also compares the fatigue suppression performance of GPL with SWNT and MWNT additives at the same nanofiller weight fraction of 0.1 ± 0.002%. The performance of the GPL is clearly superior to the nanotubes particularly as the stress intensity factor amplitude (ΔK) is increased. For the case of the nanotubes, we observe a substantial degradation in the fatigue suppression with increasing ΔK (Figure 4b). This is because in the case of nanotubes the dominant toughening and fatigue suppression mechanism is crack bridging. Previous work by our group[17−19] has shown that the fatigue crack is bridged by high aspect ratio nanotubes generating a fiber-bridging zone in the wake of the crack tip. As the crack advances, energy is dissipated by the frictional pull-out of the bridging nanotubes from the epoxy matrix which slows the crack propagation speed. However, this crack-bridging effect loses effectiveness at high ΔK due to progressive shrinkage in the size of the fiber-bridging zone as ΔK is increased.[18] The fact that such behavior is not observed in GPL/epoxy nanocomposites indicates that the toughening mechanism for GPL is different from nanotubes. Unlike nanotubes, frictional pull-out of GPL from the matrix is less likely given the strong interfacial adhesion[13,16] of GPL with polymer matrices. A possible toughening mechanism for GPL is crack deflection,[29] which is the process by which an initial crack tilts and twists when it encounters a rigid inclusion. This generates an increase in the total fracture surface area resulting in greater energy absorption as compared to the unfilled polymer material. The tilting and twisting of the crack front as it is forced to move out of the initial propagation plane also forces the crack to grow locally under mixed-mode (tensile/in-plane shear and tensile/antiplane shear) conditions. Crack propagation under mixed-mode conditions requires a higher driving force than in mode I (tension), which also results in higher fracture toughness of the material. Crack deflection processes may be highly effective for GPL given its planar (two-dimensional) geometry and large aspect ratio. The fatigue suppression response for the GPL/epoxy nanocomposite shown in Figure 4b is consistent with crack deflection,[29] although more in-depth fractography analysis is required to establish this and to investigate other possible toughening mechanisms in graphene-based materials. The test data plotted in Figures 3 and 4 are presented in tabular form in the Supporting Information.

CONCLUSION

In summary, we show that at low nanofiller content graphene platelets perform significantly better than carbon nanotubes in terms of enhancing a variety of mechanical properties including tensile strength, Young's modulus, fracture toughness, fracture energy, and resistance to fatigue crack growth. There are several possible reasons for this, which include enhanced specific area of graphene platelets, improved mechanical interlocking/adhesion at the nanofiller−matrix interface, and the two-dimensional geometry of graphene platelets. Further comparative study of carbon nanotube, nanoparticle, and graphene-based composites over a range of weight fractions is warranted to help uncover these effects.

MATERIALS AND METHODS

SWNTs and MWNTs were purchased from Cheap Tube Inc. (USA) and Nanocyl (Belgium). Natural graphite flakes with an average diameter of 48 μm were supplied from Huadong Graphite Factory (Pingdu, China). Concentrated sulfuric acid (95−98%), concentrated nitric acid (68%), and hydrochloric acid (36−38%) were purchased from Beijing Chemical Factory, China. Potassium chlorate (99.5%) was provided from Fuchen Chemical Reagents (Tianjin, China). The epoxy used in the present study was a bisphenol-A-based epoxy (Epoxy 2000 from Fibreglast, USA), and the curing agent used was 2120 Epoxy Hardener from Fibreglast, USA.

GPL Fabrication: Graphite oxide was prepared by oxidizing graphite in a solution of sulfuric acid, nitric acid, and potassium chlorate for 96 h.[14,15] Thermal exfoliation of graphite oxide was achieved by placing the graphite oxide powder (200 mg) in a 200 mm inner diameter, 1 m long quartz tube that was sealed at one end. The other end of the quartz tube was closed using a rubber stopper. An argon inlet was then inserted through the rubber stopper. The sample was flushed with argon for 10 min, and the quartz tube was quickly inserted into a tube furnace (Thermolyne 79300, Thermo Fisher Scientific Inc., USA) preheated to 1050 °C and held in the furnace for 30 s.

Dispersion of GPL in Epoxy Matrix: GPL was dispersed in acetone (100 mL of acetone to 0.1 g of GPL) using an ultrasonic probe sonicator at high amplitude (Sonics Vibracell VC 750, Sonics and Materials Inc., USA) for 1.5 h in an ice bath. The epoxy (System 2000 Epoxy Resin, Fibreglast Inc., USA) was added to the mixture and sonicated following the same procedure for another 1.5 h. Next, the acetone is evaporated off by heating the mixture on a magnetic stir plate using a Teflon-coated magnetic bar for 3 h at 70 °C. The mixture is placed in a vacuum chamber for 12 h at 70 °C to ensure that all of the acetone has been removed. After allowing the GPL/epoxy slurry to cool down to room temperature to prevent any premature curing, a low viscosity curing agent (2120 Epoxy Hardener, Fibreglast Inc., USA) was added and mixed using a high speed shear mixer (ARE-250, Thinky, Japan) for 4 min at 2000 rpm. The mixture is again placed in a vacuum chamber to degas the epoxy for approximately 30 min. Finally, the mixture is poured into silicon molds, and the nanocomposite is cured at room temperature and 90 psi pressure for 24 h, followed by 4 h of post-cure at 90 °C.

Estimation of Fracture Toughness: The mode I fracture toughness (K_{Ic}) was calculated using ASTM Standard D5045 as follows: $K_{Ic} = (P_{max}/BW^{1/2})f(a/W)$, where P_{max} is the maximum load on the load−displacement curve for the compact tension specimen, B is the thickness of the specimen, W is the width of the specimen, and $f(a/W)$ is related to the geometry of the sample. Note that, in all of our samples, the term a/W is equal to 0.5. For compact tension samples, f can be expressed as

$$f\left(\frac{a}{W}\right) = \left[\left(2 + \frac{a}{W}\right)\left(0.886 + 4.64\left(\frac{a}{W}\right) - 13.32\left(\frac{a}{W}\right)^2 + 14.72\left(\frac{a}{W}\right)^3 - 5.6\left(\frac{a}{W}\right)^4\right)\right]/\left(1 - \frac{a}{W}\right)^{3/2}$$

Fatigue Crack Propagation Testing: Fatigue tests were conducted using a MTS-858 material testing system following ASTM standard E647. An initial precrack was created in the compact tension samples by gently tapping a fresh razor blade over a molded starter notch. All tests were performed under load control at a constant load ratio R of 0.1 ($R = K_{min}/K_{max}$) and at a test frequency of 5 Hz. The crack length was measured using the compliance method and was confirmed by a high-resolution video monitoring system. For the compact tension samples tested in this study, the stress intensity factor amplitude (ΔK) was obtained as follows:

$$\Delta K = \frac{\Delta P}{BW^{1/2}} \frac{(2+\alpha)}{(1-\alpha)^{1.5}}(0.886 + 4.64\alpha - 13.32\alpha^2 + 14.72\alpha^3 - 5.6\alpha^4)$$

where ΔP is the load amplitude, $\alpha = a/W$, a is the distance between the crack tip and the loading line, W is the compact tension specimen width, and B is the specimen thickness.

X-ray Diffraction (XRD) Study of Graphite and Graphite Oxide: A Rigaku D/Max 2500 XRD with Cu Kα radiation (λ = 1.54 Å) at a generator voltage of 40 kV and a generator current of 50 mA was used to measure the diffraction behavior of natural graphite and graphite oxide (see Supporting Information). All experiments were carried out in the reflection mode at ambient temperature with 2θ varying between 1 and 30°. The scanning speed was 2.4°/min, and the step size was 0.002°.

Acknowledgment. N.K. acknowledges funding support from the U.S. Office of Naval Research (Award Number N000140910928) and the U.S. National Science Foundation (Award 0900188).

Supporting Information Available: Test data for Young's modulus, ultimate tensile strength, fracture toughness, and fracture energy are presented in tabular form. X-ray diffraction study of graphite and graphite oxide is also provided. This material is available free of charge *via* the Internet at http://pubs.acs.org.

REFERENCES AND NOTES

1. Park, S.; Ruoff, R. S. Chemical Methods for the Production of Graphenes. *Nat. Nanotechnol.* **2009**, *4*, 217–224.
2. Eizenberg, M.; Blakely, J. M. Carbon Monolayer Phase Condensation on Ni(111). *Surf. Sci.* **1970**, *82*, 228–236.
3. Aizawa, T.; Souda, R.; Otani, S.; Ishizawa, Y.; Oshima, C. Anomalous Bond of Monolayer Graphite on Transition-Metal Carbide Surfaces. *Phys. Rev. Lett.* **1990**, *64*, 768–771.
4. Berger, C.; Song, Z.; Li, X.; Wu, X.; Brown, N.; Naud, C.; Mayou, D.; Li, T.; Hass, J.; Marchenkov, A. N.; Conrad, E. H.; First, P. N.; De Heer, W. A. Electronic Confinement and Coherence in Patterned Epitaxial Graphene. *Science* **2006**, *312*, 1191–1196.
5. Novoselov, K. S.; Geim, A. K.; Morozov, S. V.; Jiang, D.; Zhang, Y.; Dubonos, S. V.; Grigorieva, I. V.; Firsov, A. A. Electric Field Effect in Atomically Thin Carbon Films. *Science* **2004**, *306*, 666–669.
6. Stankovich, S.; Piner, R. D.; Nguyen, S.-T.; Ruoff, R. S. Synthesis and Exfoliation of Isocyanate Treated Graphene Oxide Nano-platelets. *Carbon* **2006**, *44*, 3342–3347.
7. Stankovich, S.; Piner, R. D.; Chen, X.; Wu, N.; Nguyen, S. T.; Ruoff, R. S. Stable Aqueous Dispersions of Graphitic Nanoplatelets *via* the Reduction of Exfoliated Graphite

Oxide in the Presence of Poly(sodium 4-styrenesulfonate). *J. Mater. Chem.* **2006**, *16*, 155–158.
8. Brodie, B. C. Sur le Poids Atomique du Graphite. *Ann. Chim. Phys.* **1860**, *59*, 466–472.
9. Staudenmaier, L. Verfahren zur Darstellung der Graphitsaure. *Ber. Dtsch. Chem. Ges.* **1898**, *31*, 1481–1499.
10. Hummers, W. S.; Offeman, R. E. Preparation of Graphitic Oxide. *J. Am. Chem. Soc.* **1958**, *80*, 1339.
11. Boehm, H. P.; Clauss, A.; Fischer, G. O.; Hofmann, U. Das Adsorptionsverhalten Sehr Dunner Kohlenstoff-Folien. *Anorg. Allg. Chem.* **1962**, *316*, 119–127.
12. Boehm, H. P.; Eckel, M.; Scholz, W. Uber den Bildungsmechanismus des Graphitoxids. *Anorg. Allg. Chem.* **1967**, *353*, 236–242.
13. Stankovich, S.; Dikin, D. A.; Dommett, D.; Kohlhaas, K.; Zimney, E. J.; Stach, E. A.; Piner, R. D.; Nguyen, S. T.; Ruoff, R. S. Graphene-Based Composite Materials. *Nature* **2006**, *442*, 282–286.
14. Schniepp, H. C.; Li, J.-L.; McAllister, M. J.; Sai, H.; Herrera-Alonso, M.; Adamson, D. H.; Prud'homme, R. K.; Car, R.; Saville, D. A.; Aksay, I. A. Functionalized Single Graphene Sheets Derived from Splitting Graphite Oxide. *J. Phys. Chem. B.* **2006**, *110*, 8535–8539.
15. McAllister, M. J.; Li, J.-L.; Adamson, D. H.; Schniepp, H. C.; Abdala, A. A.; Liu, J.; Herrera-Alonso, M.; Milius, D. L.; Car, R.; Prud'homme, R. K.; Aksay, I. A. Single Sheet Functionalized Graphene by Oxidation and Thermal Expansion of Graphite. *Chem. Mater.* **2007**, *19*, 4396–4404.
16. Ramanathan, T.; Abdala, A. A.; Stankovich, S.; Dikin, D. A.; Herrera-Alonso, M.; Piner, R. D.; Adamson, D. H.; Schniepp, H. C.; Chen, X.; Ruoff, R. S.; Nguyen, S. T.; Aksay, I. A.; Prud'homme, R. K.; Brinson, L. C. Functionalized Graphene Sheets for Polymer Nanocomposites. *Nat. Nanotechnol.* **2008**, *3*, 327–331.
17. Zhang, W.; Srivastava, I.; Zhu, Y.-F.; Picu, C. R.; Koratkar, N. Heterogeneity in Epoxy Nanocomposites Initiates Crazing: Significant Improvements in Fatigue Resistance and Toughening. *Small* **2009**, *5*, 1403–1407.
18. Zhang, W.; Picu, C. R.; Koratkar, N. Suppression of Fatigue Crack Growth in Carbon Nanotube Composites. *Appl. Phys. Lett.* **2007**, *91*, 193109.
19. Zhang, W.; Picu, C. R.; Koratkar, N. Effect of Carbon Nanotube Dimensions and Dispersion on the Fatigue Behavior of Epoxy Nanocomposites. *Nanotechnology* **2008**, *19*, 285709.
20. Mallick, P. K. *Fiber-Reinforced Composites*; Dekker: New York, 1993; p 130.
21. Qian, D.; Dickey, E. C.; Andrews, R.; Rantell, T. Load Transfer and Deformation Mechanisms in Carbon Nanotube−Polystyrene Composites. *Appl. Phys. Lett.* **2000**, *76*, 2868–2870.
22. Zhou, X.; Shin, E.; Wang, K. W.; Bakis, C. E. Interfacial Damping Characteristics of Carbon Nanotube-Based Composites. *Compos. Sci. Technol.* **2004**, *64*, 2425–2437.
23. Thostenson, E. T.; Chou, T.-W. On the Elastic Properties of Carbon Nanotube-Based Composites: Modelling and Characterization. *J. Phys. D: Appl. Phys.* **2003**, *36*, 573–582.
24. Halpin, J. C.; Tsai, S. W. Environmental Factors in Composite Materials Design. *U.S. Air Force Technical Report AFML TR*, **1967**; pp 67−423.
25. Halpin, J. C.; Thomas, R. Ribbon Reinforcement of Composites. *J. Compos. Mater.* **1968**, *2*, 488–497.
26. Gojny, F. H.; Wichmann, M. H. G.; Kopke, U.; Fiedler, B.; Schulte, K. Carbon Nanotube-Reinforced Epoxy-Composites: Enhanced Stiffness and Fracture Toughness at Low Nanotube Content. *Compos. Sci. Technol.* **2004**, *64*, 2363–2371.
27. Blackman, B. R. K.; Kinloch, A. J.; Sohn Lee, J.; Taylor, A. C.; Agarwal, R.; Schueneman, G.; Sprenger, S. The Fracture and Fatigue Behavior of Nano-Modified Epoxy Polymers. *J. Mater. Sci.* **2007**, *42*, 7049–7051.
28. Becker, O.; Varley, R.; Simon, G. Morphology, Thermal Relaxations and Mechanical Properties of Layered Silicate Nanocomposites. *Polymer* **2002**, *43*, 4365–4373.
29. Wetzel, B.; Rosso, P.; Haupert, F.; Friedrich, K. Epoxy Nanocomposites—Fracture and Toughening Mechanisms. *Eng. Fract. Mech.* **2006**, *73*, 237.